Triangle–hinge models for unoriented membranes

AUTHOR(S):

Fukuma, Masafumi; Sugishita, Sotaro; Umeda, Naoya

CITATION:

Fukuma, Masafumi ...[et al]. Triangle–hinge models for unoriented membranes. Progress of Theoretical and Experimental Physics 2016, 2016(7): 073B01.

ISSUE DATE:

2016-07-12

URL:

http://hdl.handle.net/2433/216698

PTEP

Prog. Theor. Exp. Phys. **2016**, 073B01 (24 pages)
DOI: 10.1093/ptep/ptw069

Triangle–hinge models for unoriented membranes

Masafumi Fukuma*, Sotaro Sugishita*,† and Naoya Umeda*

Department of Physics, Kyoto University, Kyoto 606-8502, Japan
†*Present address: Department of Physics, Osaka University, Toyonaka 560-0043, Japan*
*E-mail: fukuma@gauge.scphys.kyoto-u.ac.jp, sugishita@het.phys.sci.osaka-u.ac.jp, n_umeda@gauge.scphys.kyoto-u.ac.jp

Received March 17, 2016; Accepted April 14, 2016; Published July 12, 2016

Triangle–hinge models [M. Fukuma, S. Sugishita, and N. Umeda, J. High Energy Phys. **1507**, 088 (2015)] are introduced to describe worldvolume dynamics of membranes. The Feynman diagrams consist of triangles glued together along hinges and can be restricted to tetrahedral decompositions in a large-N limit. In this paper, after clarifying that all the tetrahedra resulting in the original models are orientable, we define a version of triangle–hinge models that can describe the dynamics of *unoriented* membranes. By regarding each triangle as representing a propagation of an open membrane of disk topology, we introduce a local worldvolume parity transformation which inverts the orientation of a triangle, and define unoriented triangle–hinge models by gauging the transformation. Unlike two-dimensional cases, this local transformation generally relates a manifold to a nonmanifold, but still is a well-defined manipulation among tetrahedral decompositions. We further show that matter fields can be introduced in the same way as in the original oriented models. In particular, the models will describe unoriented membranes in a target spacetime by taking matter fields to be the target space coordinates.

Subject Index B25, B83, B86, E05

1. Introduction

The worldvolume theory of membranes in a spacetime is equivalent to a system of three-dimensional quantum gravity coupled to matter fields corresponding to the target space coordinates. One approach to treating such a class of systems is the use of models that generate three-dimensional random volumes. Triangle–hinge models [1] are proposed as such models. The dynamical variables are given by a pair of $N \times N$ symmetric matrices, A and B, and the Feynman diagrams consist of triangles glued together along their edges. We can restrict the diagrams such that they represent only three-dimensional tetrahedral decompositions by taking a large-N limit. The simplest model thus obtained corresponds to discretized three-dimensional pure quantum gravity with a bare cosmological constant. We can further introduce extra degrees of freedom representing the target space coordinates. A prescription to introduce such matter degrees of freedom to triangle–hinge models is given in [2]. The prescription also enables us to describe various spin systems such as the q-state Potts models coupled to quantum gravity, and to realize colored tensor models [3,4] in terms of triangle–hinge models.

As pointed out in [1], the original triangle–hinge models generate only (and all of the) orientable tetrahedral decompositions. In this paper, we generalize the models such that unoriented membranes can be treated. We will call the obtained models *unoriented triangle–hinge models*. In the context of

Funded by SCOAP[3]

string theory, to consider unoriented models is not just interesting as a mathematical generalization, but has a physically important meaning. Actually, an unoriented superstring theory, type I superstring, is one of the (perturbatively) consistent superstring theories. We expect that unoriented membrane theory is also physically important.[1]

In two-dimensional cases, an unoriented theory is obtained by gauging the worldsheet parity of an oriented theory. If we discretize worldsheets by triangular decompositions, the gauging procedure is to treat equally two ways to identify an edge of a triangle with that of another triangle; one way preserves the local orientations of two triangles and the other does not. We will define unoriented membrane theories by generalizing the prescription to three-dimensional tetrahedral decompositions. Roughly speaking, the unoriented models equally treat two possible ways to identify a triangle of a tetrahedron with that of another tetrahedron; one way preserves the orientation and the other does not.

Here, we comment on the treatment of orientability in other three-dimensional random volume theories, tensor models. Tensor models [5–7] are natural generalizations of matrix models to higher dimensions. One can introduce various kinds of tensor models [6] depending on how indices of rank-3 tensors are assigned to triangles in tetrahedral decompositions.[2] A class of models where each index is assigned to a vertex of a triangle generate only orientable tetrahedral decompositions [6]. Although we may be able to construct unoriented models by modifying the models, it is difficult to solve them. Analytical treatment of tensor models is improved in colored tensor models [3,4]. The models only generate tetrahedral decompositions belonging to a specific class.[3] This restriction enables us to take a $1/N$ expansion of the free energy [14,15]. Furthermore, in the so-called invariant models [16] one can take the double scaling limit [17,18]. It can be shown that tetrahedral decompositions generated by colored tensor models are orientable. However, if we try to modify the models to unoriented ones, the solvability of the models may be lost.

The original triangle–hinge models are expected to be solvable because the dynamical variables are matrices. In fact, for simple models (such as the models characterized by matrix rings), the interaction terms in the action can be rewritten to the traces of powers of matrices (M. Fukuma, S. Sugishita, and N. Umeda, in preparation). Thus, in order to reduce the systems to those of eigenvalues, we only need to integrate the exponential of the quadratic term in the action over the angular parts of matrices. Moreover, numerical integrations (M. Fukuma, S. Sugishita, and N. Umeda, in preparation) show that the eigenvalue distributions of matrices A and B have a similar structure to those of one-matrix models with double-well potentials, and that the effective theory of eigenvalues for either of matrix A or B has critical points. Since there are integration contours for which the matrix integrations are finite (M. Fukuma, S. Sugishita, and N. Umeda, in preparation), it is highly expected that the original oriented triangle–hinge models have well-defined continuum limits. We will see that the actions of unoriented triangle–hinge models have a similar structure to the original ones, and thus we expect

[1] We should comment that the low-energy effective theory of unoriented supermembranes is not 11-dimensional supergravity, because the three-form fields in the supergravity multiplet cannot couple to unoriented membranes. Nevertheless, we expect that unoriented membrane theory serves as a toy model to obtain a better understanding of dynamics of membranes.

[2] There is another type of tensor model (called the canonical tensor model) which realizes the constraints in the canonical quantization of gravity [8–10]. An interesting connection to random tensor networks is studied in [11,12].

[3] See, e.g., [13] for an attempt to relax the restriction on the diagrams generated in colored tensor models.

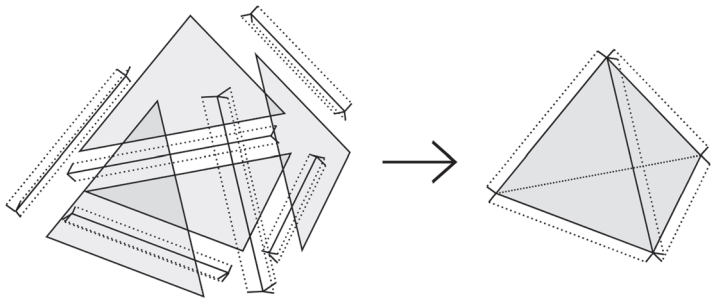

Fig. 1. Part of a configuration consisting of triangles glued together with multiple hinges [1].

that unoriented triangle–hinge models are also solvable and might be easier to solve due to the higher symmetry they have.

This paper is organized as follows. In Sect. 2, we review triangle–hinge models and show that the tetrahedral decompositions generated by the models are orientable. In Sect. 3, after reviewing matrix models for unoriented strings, we define unoriented membrane theories in terms of tetrahedral decompositions. In Sect. 4, we give a version of triangle–hinge models that realizes unoriented membrane theories. In Sect. 5, we show that matter fields can also be introduced to unoriented triangle–hinge models by the same procedure as [2]. Section 6 is devoted to our conclusions.

2. Orientability in triangle–hinge models

In this section, we clarify the fact that the original triangle–hinge model [1] generates the set of *oriented* tetrahedral decompositions.

2.1. Brief review of triangle–hinge models

Triangle–hinge models [1] are designed to generate Feynman diagrams each of which can be regarded as a collection of triangles glued together along multiple hinges and will eventually give a three-dimensional tetrahedral decomposition in a large-N limit (see Fig. 1).[4]

The dynamical variables are given by a pair of $N \times N$ real symmetric matrices, $A = (A_{ij} = A_{ji})$ and $B = (B^{ij} = B^{ji})$, and the action takes the form[5]

$$\begin{aligned} S[A,B] &= \frac{1}{2}\,[AB] - \frac{\lambda}{6}\,[CAAA] - \sum_{k\geq 1}\frac{\mu_k}{2k}\,[Y_k \underbrace{B\cdots B}_{k}] \\ &\equiv \frac{1}{2}\,A_{ij}B^{ij} - \frac{\lambda}{6}\,C^{i_1j_1i_2j_2i_3j_3}A_{i_1j_1}A_{i_2j_2}A_{i_3j_3} - \sum_{k\geq 1}\frac{\mu_k}{2k}\,Y_{i_1j_1\ldots i_kj_k}B^{i_1j_1}\cdots B^{i_kj_k}. \end{aligned} \tag{2.1}$$

The free energy is given by

$$F = \log\int dA\,dB\,e^{-S[A,B]}, \tag{2.2}$$

and if we expand F with respect to λ and μ_k, each term is expressed by a group of Wick contractions as usual. There are two types of interaction vertices: one (coming from $\lambda\,[CA^3]$) corresponds to a triangle, and the other (coming from $\mu_k[Y_kB^k]$) to a multiple hinge (see Fig. 2). The coefficients

[4] Here, a (multiple) hinge is an object connecting edges of triangles. A hinge with k edges is called a k-hinge.
[5] Note that we have included in the action the interaction term corresponding to 1-hinges.

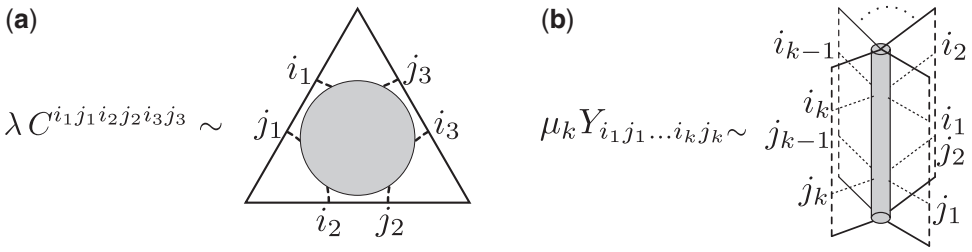

Fig. 2. Interaction vertices corresponding to (a) triangles and (b) k-hinges [1].

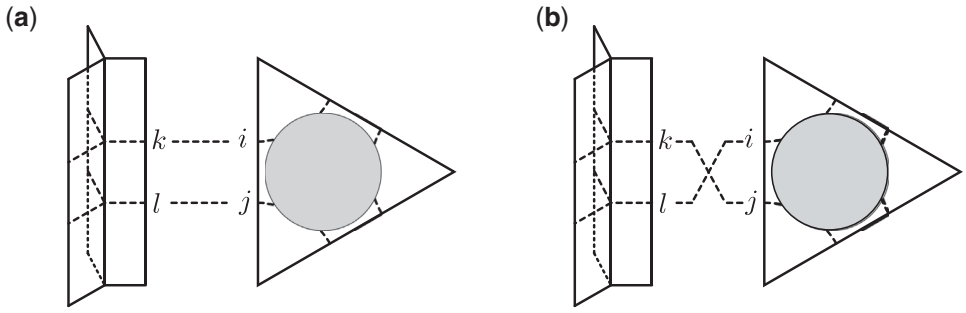

Fig. 3. Two ways to connect an edge of a triangle to an edge of a hinge. If we fix the position of the triangle, (b) represents the diagram where the edge of the hinge is glued to that of the triangle upside down compared to (a).

C^{ijklmn} and $Y_{i_1 j_1 \ldots i_k j_k}$ are real constant tensors, and we will not assume any symmetry for the indices of $C^{i_1 j_1 i_2 j_2 i_3 j_3}$ and $Y_{i_1 j_1 \ldots i_k j_k}$ until we give their explicit forms later [see (2.12) and (2.10)].[6] They are connected by a free propagator

$$\overbrace{A_{ij} B^{kl}} = \delta_i^k \delta_j^l + \delta_i^l \delta_j^k . \tag{2.3}$$

The two terms on the right-hand side in (2.3) express that there are two ways to connect an edge of a hinge to an edge of a triangle, as shown in Fig. 3. We regard the two types of pairing as representing two independent Wick contractions and write the first type as $\overbrace{AB}^{(+)}$, or simply as $AB^{(+)}$, and the second type as $\overbrace{AB}^{(-)} = AB^{(-)}$, where we have omitted the indices $i, j, \ldots$.[7] Then, a group of Wick contractions (denoted by x) can be specified uniquely in a form such as

$$x = [CA_1A_2A_3]\,[CA_4A_5A_6] \cdots [Y_k B_1^{(+)} B_6^{(-)} \cdots]\,[Y_{k'} B_5^{(+)} \cdots] \cdots , \tag{2.4}$$

where the subscript I of A_I and $B_I^{(\pm)}$ indicates that they belong to the Ith contraction of type $\overbrace{AB}^{(\pm)}$. As explained above, we do not impose a symmetry for the coefficients C and Y, and think that

[6] In fact, when multiplied by $A_{i_1 j_1} A_{i_2 j_2} A_{i_3 j_3}$ ($A_{ij} = A_{ji}$), only fully symmetric parts of $C^{i_1 j_1 i_2 j_2 i_3 j_3}$ survive that are invariant under interchanges of indices i_α and j_α ($\alpha = 1, \ldots, 3$) and under permutations of three pairs of indices $(i_1 j_1)$, $(i_2 j_2)$, $(i_3 j_3)$, so we could have assumed that the tensor C in (2.1) has the symmetry $C^{i_1 j_1 i_2 j_2 i_3 j_3} = C^{i_2 j_2 i_3 j_3 i_1 j_1} = C^{j_1 i_1 i_2 j_2 i_3 j_3} = C^{i_2 j_2 i_1 j_1 i_3 j_3}$. However, we do not assume this symmetry and regard contractions using $C^{i_1 j_1 i_2 j_2 i_3 j_3}$, $C^{i_2 j_2 i_3 j_3 i_1 j_1}$, $C^{j_1 i_1 i_2 j_2 i_3 j_3}$, or $C^{i_2 j_2 i_1 j_1 i_3 j_3}$ as giving independent Wick contractions [1,2]. Note that only the fully symmetric part is actually left when all the diagrams are summed. The same argument is applied to the hinge parts.

[7] Of course, the two pairs appear in a combined way as $\overbrace{AB}^{(+)} + \overbrace{AB}^{(-)}$.

changing the order of the labels in $[CA^3]$ or $[Y_kB^k]$ (e.g., replacing $[CA_1A_2A_3]$ by $[CA_2A_3A_1]$) leads to a different group of Wick contractions.

In [1], we investigated in detail the case where the interaction terms $\mu_k[Y_kB^k]$ are characterized by a semisimple associative algebra $\mathcal{A}$. Let a basis of $\mathcal{A}$ be $\{e_i\}$ $(i = 1, \ldots, N)$, where N is the dimension of $\mathcal{A}$ as a linear space. The multiplication $\times$ of $\mathcal{A}$ is then specified by the structure constants $y_{ij}{}^k$ as

$$e_i \times e_j = y_{ij}{}^k e_k \,. \tag{2.5}$$

We further introduce a rank-k tensor from the structure constants as[8]

$$y_{i_1 \ldots i_k} = y_{i_1 j_1}{}^{j_k} y_{i_2 j_2}{}^{j_1} \cdots y_{i_k j_k}{}^{j_{k-1}}, \tag{2.6}$$

which enjoys the cyclic symmetry $y_{i_1 \ldots i_k} = y_{i_2 \ldots i_k i_1}$. Then the coupling constants $Y_{i_1 j_1 \ldots i_k j_k}$ associated with hinges are defined to be

$$Y_{i_1 j_1 \ldots i_k j_k} \equiv y_{i_1 \ldots i_k} y_{j_k \ldots j_1} \,, \tag{2.7}$$

which enjoy the symmetry properties

$$Y_{i_1 j_1 \ldots i_k j_k} = Y_{i_2 j_2 \ldots i_k j_k i_1 j_1} = Y_{j_k i_k \ldots j_1 i_1} \,. \tag{2.8}$$

In order to restrict configurations so as to represent only tetrahedral decompositions, we consider the case where the algebra $\mathcal{A}$ is a matrix ring $\mathcal{A} = M_{n=3m}(\mathbb{R})$ with n being a multiple of three [1]. The dimension of $\mathcal{A}$ is then given by $N = n^2 = (3m)^2$. We take a basis $\{e_i\}$ to be $\{e_{ab}\}$ $(a, b = 1, \ldots n)$, where e_{ab} are the matrix units whose (c, d) elements are $(e_{ab})_{cd} = \delta_{ac}\delta_{bd}$. Note that indices i are replaced by double indices ab. Then, the rank-k tensors (2.6) are given by

$$y_{i_1 i_2 \ldots i_k} = y_{a_1 b_1, a_2 b_2, \ldots, a_k b_k} = n\, \delta_{b_1 a_2} \cdots \delta_{b_{k-1} a_k} \delta_{b_k a_1} \,, \tag{2.9}$$

which in turn give the k-hinge tensor $Y_{i_1 j_1 i_2 j_2 \ldots i_k j_k}$ as

$$Y_{a_1 b_1 c_1 d_1, a_2 b_2 c_2 d_2, \ldots, a_k b_k c_k d_k} = n^2\, \delta_{b_1 a_2} \cdots \delta_{b_{k-1} a_k} \delta_{b_k a_1}\, \delta_{c_1 d_2} \cdots \delta_{c_{k-1} d_k} \delta_{c_k d_1} \,. \tag{2.10}$$

We further introduce a permutation matrix ω of the following form:

$$\omega = \begin{pmatrix} 0 & 1_{n/3} & 0 \\ 0 & 0 & 1_{n/3} \\ 1_{n/3} & 0 & 0 \end{pmatrix}, \qquad 1_m : m \times m \text{ unit matrix}, \tag{2.11}$$

and set the tensor $C^{i_1 j_1 i_2 j_2 i_3 j_3}$ in (2.1) to be

$$C_+^{a_1 b_1 c_1 d_1, a_2 b_2 c_2 d_2, a_3 b_3 c_3 d_3} \equiv \frac{1}{n^3}\, \omega^{d_1 a_2} \omega^{d_2 a_3} \omega^{d_3 a_1} \omega^{b_3 c_2} \omega^{b_2 c_1} \omega^{b_1 c_3} . \tag{2.12}$$

[8] The rank-one tensor y_i is especially defined as $y_i = y_{ij}{}^j$.

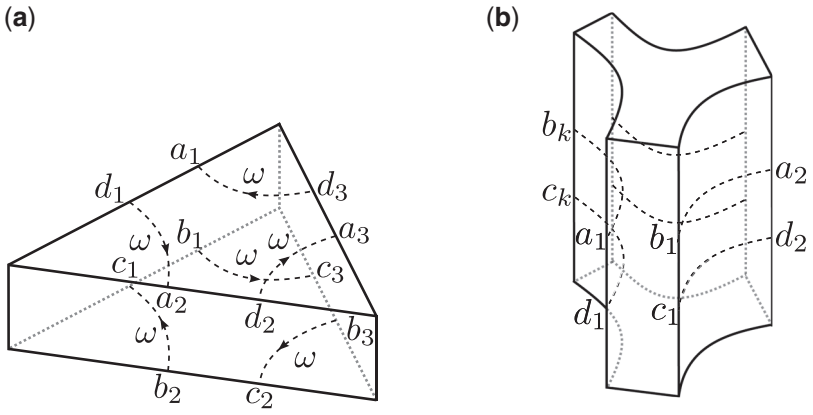

Fig. 4. (a) Thickened triangles; (b) thickened hinges [1]. Each thickened triangle has six index lines with arrows corresponding to ω.

Note that C_+ enjoys the symmetry properties

$$C_+^{i_1j_1i_2j_2i_3j_3} = C_+^{i_2j_2i_3j_3i_1j_1} = C_+^{j_3i_3j_2i_2j_1i_1} . \tag{2.13}$$

The action then takes the form

$$\begin{aligned} S &= \frac{1}{2}[AB] - \frac{\lambda}{6}[C_+AAA] - \sum_{k\geq 1}\frac{\mu_k}{2k}[Y_k \underbrace{B\cdots B}_{k}] \\ &\equiv \frac{1}{2}A_{abcd}B_{abcd} \\ &\quad - \frac{\lambda}{6n^3}\omega^{d_1a_2}\omega^{d_2a_3}\omega^{d_3a_1}\omega^{b_3c_2}\omega^{b_2c_1}\omega^{b_1c_3}A_{a_1b_1c_1d_1}A_{a_2b_2c_2d_2}A_{a_3b_3c_3d_3} \\ &\quad - \sum_{k\geq 1}\frac{n^2\mu_k}{2k}B_{a_1a_2b_2b_1}\cdots B_{a_{k-1}a_kb_kb_{k-1}}B_{a_ka_1b_1b_k} . \end{aligned} \tag{2.14}$$

The interaction vertices can be represented by thickened triangles and hinges (see Fig. 4), and are connected with the use of two types of Wick contractions between A_{abcd} and B_{efgh},

$$\overbrace{AB}^{(+)} = \delta_{ae}\delta_{bf}\delta_{cg}\delta_{dh} , \qquad \overbrace{AB}^{(-)} = \delta_{ag}\delta_{bh}\delta_{ce}\delta_{df} . \tag{2.15}$$

Note that arrows are assigned to index lines on triangles, as in Fig. 4, and that their directions are preserved when two triangles are glued together along an intermediate hinge (see Fig. 5).

We introduce here some terminology to discriminate between a group of Wick contractions and a Feynman diagram. We have already clarified our rule about Wick contractions. We now introduce an equivalence relation to the set $\{x\}$ of groups of Wick contractions, saying that a group x of Wick contractions is equivalent to another group y (and writing $x \sim y$) if x is obtained from y by repetitive use of the relations (2.8) and (2.13) and by permuting interaction vertices of the same type. We denote the equivalence class of x by $[x] = \{y \,|\, y \sim x\}$, and call $\gamma = [x]$ a Feynman diagram. The perturbative expansion of the free energy is then given by a sum over connected Feynman diagrams γ, $F = \sum_\gamma F(\gamma)$. In a connected diagram, every index line makes a loop since all the indices are contracted.

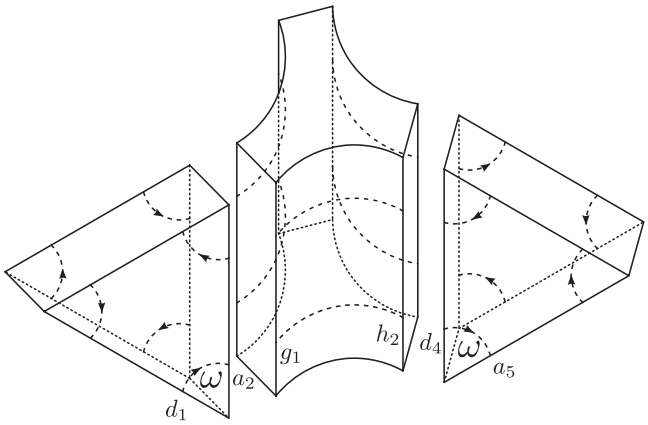

Fig. 5. Gluing of thickened triangles along a hinge. Indices a_2 and d_4 are contracted with g_1 and h_2, respectively, giving $(\omega^2)^{d_1 a_5}$.

2.2. Restriction to tetrahedral decompositions

Although configurations generated in triangle–hinge models do not generally represent tetrahedral decompositions, the set of Feynman diagrams can be reduced such that they represent only (and all of the) tetrahedral decompositions if we take a large-n limit with n/λ and $n^2\mu_k$ fixed [1].[9] The point is the following. We have $\mathrm{tr}\,\omega^\ell$ when ω appears ℓ times in an index loop (see Fig. 5), and thus $F(\gamma)$ is given by

$$F(\gamma) = \frac{1}{S(\gamma)}\left(\frac{\lambda}{n^3}\right)^{s_2(\gamma)}\left[\prod_{k=1}(n^2\mu_k)^{s_1^k(\gamma)}\right]\prod_{\ell=1}[\mathrm{tr}\,\omega^\ell]^{t_2^\ell(\gamma)}. \tag{2.16}$$

Here, $t_2^\ell(\gamma)$ denotes the numbers of index ℓ-gons in diagram γ;[10] $s_2(\gamma)$ and $s_1^k(\gamma)$ denote the number of triangles and k-hinges in diagram γ, respectively; and $S(\gamma)$ is the symmetry factor. Due to the definition of matrix ω, we have

$$\mathrm{tr}\,\omega^\ell = \begin{cases} n & (\ell = 0 \mod 3) \\ 0 & (\ell \neq 0 \mod 3). \end{cases} \tag{2.17}$$

Thus, there can survive only the diagrams with ℓ a multiple of three ($\ell \equiv 3\ell'$), and we can assume (2.16) to take the form

$$F(\gamma) = \frac{1}{S(\gamma)}\lambda^{s_2(\gamma)}\left[\prod_{k\geq 1}(n^2\mu_k)^{s_1^k(\gamma)}\right] n^{-3s_2(\gamma)+\sum_{\ell'\geq 1} t_2^{3\ell'}(\gamma)}. \tag{2.18}$$

One can show that only the index polygons with $\ell = 3$ (i.e. $\ell' = 1$) survive in the limit $n \to \infty$ with n/λ and $n^2\mu_k$ fixed [1]. We give here a proof in a form slightly different from the original one such that it can be applied to unoriented models. We first note that the relation $\sum_{\ell'\geq 1} 3\ell' t_2^{3\ell'}(\gamma) = 6s_2(\gamma)$ holds because the left-hand side counts the number of ω in diagram γ and each thickened triangle has

[9] The set of tetrahedral decompositions can be further restricted so as to represent *manifolds* by extending the algebra $\mathcal{A}$ as having a center to count the number of vertices [1].

[10] An index loop is called an *index ℓ-gon* if it consists of ℓ intervals, each living on a side of an intermediate triangle [1].

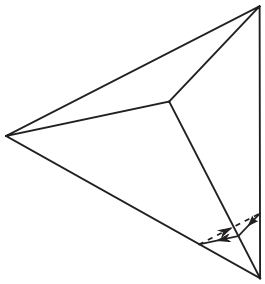

Fig. 6. An index triangle made on three sides of thickened triangles, which form a corner of a tetrahedron.

six insertions of ω. Then, if we introduce a nonnegative quantity $d(\gamma) \equiv \sum_{\ell' \geq 1} 3(\ell'-1) t_2^{3\ell'}(\gamma) \geq 0$, we have the relation $d(\gamma) = 6s_2(\gamma) - 3\sum_{\ell' \geq 1} t_2^{3\ell'}(\gamma)$. Thus, $\lambda^{s_2(\gamma)}$ can be rewritten as

$$\lambda^{s_2(\gamma)} = \lambda^{-\frac{1}{3}d(\gamma)} \lambda^{3s_2(\gamma) - \sum_{\ell' \geq 1} t_2^{3\ell'}(\gamma)} . \tag{2.19}$$

Substituting this expression into (2.18), $F(\gamma)$ is expressed as

$$F(\gamma) = \frac{1}{S(\gamma)} \lambda^{-\frac{1}{3}d(\gamma)} \left[\prod_{k \geq 1} (n^2 \mu_k)^{s_1^k(\gamma)} \right] \left(\frac{n}{\lambda} \right)^{-3s_2(\gamma) + \sum_{\ell' \geq 1} t_2^{3\ell'}(\gamma)} . \tag{2.20}$$

Therefore, in the limit $n \to \infty$ with n/λ and $n^2\mu_k$ fixed (and thus $\lambda \to \infty$), only the diagrams satisfying $d(\gamma) = 0$ can give nonzero contributions to the free energy. Since $d(\gamma) = 0$ means that all the index polygons in γ are triangles, we conclude that the large-n limit reduces the set of diagrams so that all the index polygons are triangles. One can further prove that such diagrams represent tetrahedral decompositions [1], as may be understood intuitively from the fact that if there is an index triangle, then sides of thickened triangles must be attached as in Fig. 6.[11]

We end this subsection with a comment. The above argument can also be applied to the unoriented models to be defined in the next section. Namely, if a set of diagrams is reduced such that all the index polygons are triangles, then the diagrams represent tetrahedral decompositions even for unoriented models.

2.3. *Orientability*

It is pointed out in [1] that all the tetrahedral decompositions generated by the action (2.14) are orientable. We give here a detailed proof of this statement, by clarifying the definition of orientation for Feynman diagrams in a triangle–hinge model.

We first recall that a thickened triangle has two triangular sides, on each of which directed index lines are drawn [see Fig. 4(a)]. Given a tetrahedron T formed by four triangular sides (each coming from a thickened triangle), we embed it in a three-dimensional Euclidean space E^3 as a regular tetrahedron of unit volume. Note that there can be two embeddings f^+ and f^- (up to rotations and translations in E^3), depending on whether the directions of the index lines are counterclockwise or clockwise when seen from the center of the embedded tetrahedron (see Fig. 7).[12] We say the former

[11] Note that there is ω at each corner of a side of a thickened triangle.

[12] Note that if the directions of the index lines are counterclockwise for one side, they are also counterclockwise for the other three sides because index lines are connected in such a way that the direction is preserved.

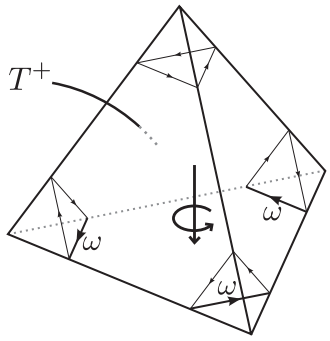

Fig. 7. A positively oriented tetrahedron T^+, corresponding to a positive embedding of T in E^3.

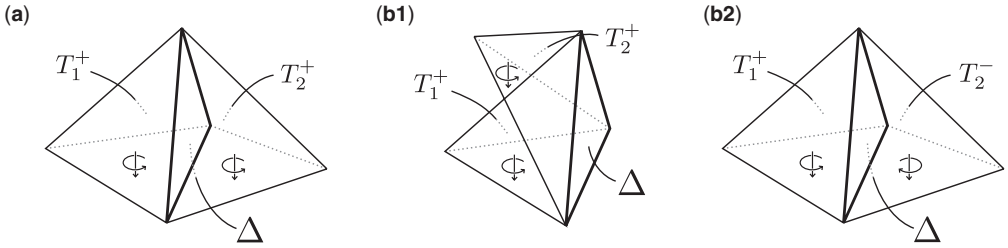

Fig. 8. Two tetrahedra T_1 and T_2 glued at triangle Δ. (a) Both tetrahedra are positively oriented, and the orientation is preserved because they are in opposite positions with respect to Δ. (b1) Both are positively oriented, but the orientation is not preserved because they are in the same position with respect to Δ. (b2) They are in opposite positions but are differently oriented.

embedding is *positive* and the latter *negative*. We then define an *oriented tetrahedron* $T^\pm$ to be the pair of tetrahedron and embedding, $T^\pm \equiv (T, f^\pm)$.

When two positively oriented tetrahedra T_1^+ and T_2^+ are glued at a triangle Δ, we say that the orientation is preserved if the two positive embeddings f_1^+ and f_2^+ can be extended (with the use of rotations and translations) to a common embedding f of $T_1^+ \cup T_2^+$ such that the images of two tetrahedra are in opposite positions with respect to the intermediate triangle Δ (see Fig. 8). We then say that a tetrahedral decomposition Γ is *orientable* if the orientation is preserved for any two adjacent tetrahedra of positive orientation.

The above orientability condition actually holds for the tetrahedral decompositions discussed in the previous subsection. In fact, the index lines on the two sides of a thickened triangle are drawn in opposite directions as in Fig. 4(a), and thus for any two adjacent tetrahedra there always exists a natural extension of their positive embeddings such that the images of two tetrahedra are in opposite positions with respect to the triangle. Since this holds for every two adjacent tetrahedra, we conclude that all the tetrahedral decompositions are orientable.

3. Unoriented membrane theories

In this section, we define unoriented membrane theories in terms of tetrahedral decompositions. A realization of unoriented membrane theories within the framework of triangle–hinge models will be given in the next section.

3.1. Matrix models for unoriented strings

As a warm-up before discussing unoriented membrane theories, we review the definition of unoriented string theories and how some of them are realized in terms of real symmetric matrix models.

We first recall that an *oriented* open string is an oriented one-dimensional object with two ends. If we forget about the target-space degrees of freedom, the scattering processes of oriented open strings are represented by Feynman diagrams of Hermitian matrix models:

$$S[M] = \mathrm{tr}\Big(\frac{1}{2}M^2 - \frac{\lambda}{3}M^3\Big), \tag{3.1}$$

where $M = (M_{ij}) = M^\dagger$ is an $N \times N$ Hermitian matrix. In fact, the propagator and the interaction vertex are expressed as[13]

$$\text{propagator}: \quad \begin{matrix} i & \text{---------} & l \\ j & \text{---------} & k \end{matrix} \sim \delta_{il}\delta_{jk} \ \big(= \overbrace{M_{ij}M_{kl}}\big), \tag{3.2}$$

$$\text{interaction}: \quad \sim \lambda\, \delta^{jk}\, \delta^{lm}\, \delta^{ni}\,. \tag{3.3}$$

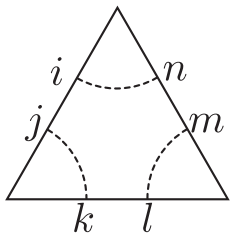

Each Feynman diagram can also be thought of as a triangular decomposition of an orientable two-dimensional surface by representing it with the dual diagram.

We now introduce a transformation Ω which acts on one-string states and inverts the worldsheet parity (the orientation of the string). *Unoriented* open string theories are then defined as theories where the transformation Ω is gauged (see, e.g., [19]). Namely, we demand that every propagator in the open-string channel be invariant under the action of Ω. This is realized by inserting the projector $(1+\Omega)/2$ to every propagator. If we do not change the form of interaction, the Feynman rules are then expressed as follows (we have rescaled the projector for later convenience):

$$\text{propagator}: \quad \begin{matrix} i & \text{---------} & l \\ j & \text{---------} & k \end{matrix} \ + \ \begin{matrix} i & \text{---}\diagdown\diagup\text{---} & l \\ j & \text{---}\diagup\diagdown\text{---} & k \end{matrix} \sim \delta_{il}\delta_{jk} + \delta_{ik}\delta_{jl} \ \big(= \overbrace{X_{ij}X_{kl}}\big), \tag{3.4}$$

[13] Note that in $\mathrm{tr}(M^3) = C^{ijklmn}M_{ij}M_{kl}M_{mn}$, only such components of C^{ijklmn} survive that are totally symmetric under the permutation of three pairs of indices, (ij), (kl), (mn). However, when we write $C^{ijklmn} = \delta^{jk}\delta^{lm}\delta^{ni}$, we intentionally think that C^{ijklmn} are only cyclically symmetric for three pairs of indices, and distinguish two diagrams, one coming from C^{ijklmn} and the other from C^{klijmn}. Of course, by summing two forms of Wick contraction in calculating the free energy, the two diagrams appear in a combined way and C^{ijklmn} will be automatically symmetrized. This "trick" enables us to identify a Feynman diagram with a triangulated surface, and is widely and implicitly adopted in the study of matrix models.

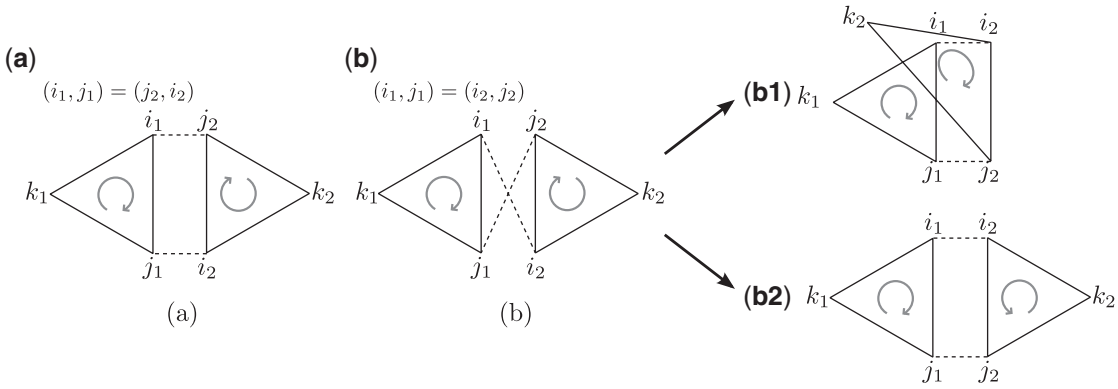

Fig. 9. Two ways to identify edges of triangles of positive orientation. The orientation is preserved for (a) $(i_1,j_1) = (j_2,i_2)$, but is not for (b) $(i_1,j_1) = (i_2,j_2)$. The local two-dimensional orientations of triangles induce one-dimensional orientations of the edges to be identified. The identification (b) can also be expressed as (b1) or (b2). The expression (b2) is necessarily accompanied by the flip of the right triangle, which means that the local two-dimensional orientation is not preserved when one moves from the left triangle to the right triangle across the identified edge.

$$\text{interaction}: \quad \begin{array}{ccc} i & & n \\ & \diagdown\!\!\diagup & \\ j & & m \\ & \diagup\!\!\diagdown & \\ k & & l \end{array} \quad \sim \lambda\, \delta^{jk}\, \delta^{lm}\, \delta^{ni}. \tag{3.5}$$

It is easy to see that the above Feynman rules are obtained from a real symmetric matrix model:

$$S = \mathrm{tr}\Big(\frac{1}{4}X^2 - \frac{\lambda}{6}X^3\Big), \tag{3.6}$$

where $X = (X_{ij}) = X^T$ is an $N \times N$ real symmetric matrix.

A Feynman diagram for the above unoriented string theory can also be represented as a collection of triangles glued together along two-hinges. In fact, if we express the vertex C^{ijklmn} (only with a cyclic symmetry) by an oriented triangle, the two contractions in (3.4) can be illustrated as in Fig. 9. The first contraction leads to a gluing of two oriented triangles with the orientation being preserved, while the second contraction leads to a gluing for which the orientation is not preserved.

3.2. Unoriented membrane theories

In the previous subsection, we have seen that unoriented string theories are obtained from oriented theories by gauging the worldsheet parity transformation Ω. We now apply the same prescription to membrane theories in order to define *unoriented membrane theories*. We first prepare oriented models and introduce the worldvolume parity transformation Ω that inverts the orientation of the open membrane, and then gauge the transformation Ω by inserting $(1 + \Omega)/2$ to every propagator of the open membrane in the original oriented models. In the rest of this paper, we assume that worldvolumes in oriented models are already represented as tetrahedral decompositions.

3.2.1. Open membranes of disk topology as fundamental objects

We first argue that the worldvolume dynamics of oriented *closed* membranes of various topologies can also be regarded as that of oriented *open membranes of disk topology*. In fact, tetrahedra in a

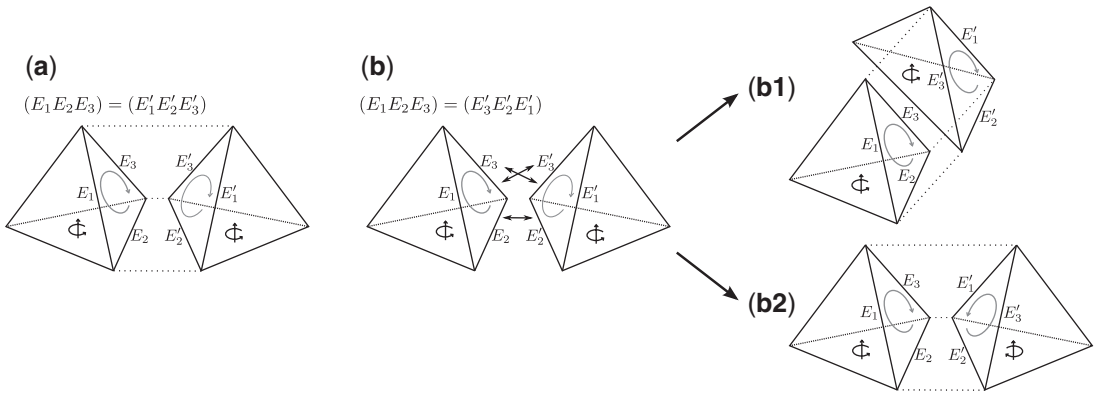

Fig. 10. Two ways to identify triangles of tetrahedra of positive orientation. The orientation is preserved for (a) $(E_1E_2E_3) = (E'_1E'_2E'_3)$, but is not for (b) $(E_1E_2E_3) = (E'_3E'_2E'_1)$. The local three-dimensional orientations of tetrahedra induce two-dimensional orientations of the triangles to be identified. The identification (b) can also be expressed as (b1) or (b2). The expression (b2) is necessarily accompanied by the orientation change of the right tetrahedron, which means that the local three-dimensional orientation is not preserved when one moves from the left tetrahedron to the right tetrahedron across the identified triangle.

tetrahedral decomposition can be thought of as interaction vertices that are connected with propagators of membranes of disk topology (i.e. triangles). One thus may say that a worldvolume theory of closed membranes of arbitrary topologies has a dual picture where open membranes of disk topology play fundamental roles, despite the fact that open membranes can have topologies other than disk (such as disks with handles).

3.2.2. Fundamental triplets for oriented membranes

Given an oriented model, we focus on two adjacent, positively oriented tetrahedra T_1^+ and T_2^+ in a tetrahedral decomposition Γ, where T_1^+ and T_2^+ are glued by identifying a triangle Δ_1 in T_1^+ with a triangle Δ_2 in T_2^+ (the resulting identified triangle will be denoted by Δ). Note that the orientation of a tetrahedron naturally induces the positive orientation for four triangles belonging to the tetrahedron, and we represent them by arrows as in Fig. 10(a). We express the identification of edges at Δ as

$$(E_1E_2E_3) = (E'_1E'_2E'_3)\,, \tag{3.7}$$

where E_1, E_2, E_3 (or E'_1, E'_2, E'_3) are the edges of Δ_1 (or Δ_2). Note that the orientations of Δ_1 and Δ_2 must be opposite in order to form an oriented tetrahedral decomposition, and thus the three-dimensional orientation is preserved when one moves from the inside of T_1 to that of T_2 through the identified triangle Δ [Fig. 10(a)]. Three-dimensional orientation is also preserved for the two other tetrahedral decompositions that are obtained from (3.7) by cyclically permuting the edges (E'_1, E'_2, E'_3). We denote by $\Gamma_1 (= \Gamma)$, Γ_2, Γ_3, respectively, the tetrahedral decompositions corresponding to the three edge-identifications that preserve the orientation,

$$\Gamma_1 : (E_1E_2E_3) = (E'_1E'_2E'_3), \quad \Gamma_2 : (E_1E_2E_3) = (E'_2E'_3E'_1), \quad \Gamma_3 : (E_1E_2E_3) = (E'_3E'_1E'_2)\,. \tag{3.8}$$

We will call $(\Gamma_1, \Gamma_2, \Gamma_3)$ the *fundamental triplet associated with triangle* Δ.

3.2.3. Definition of unoriented membrane theories

In addition to the edge-identifications (3.8) [leading to the fundamental triplet $(\Gamma_1, \Gamma_2, \Gamma_3)$], we introduce another triplet $(\tilde{\Gamma}_1, \tilde{\Gamma}_2, \tilde{\Gamma}_3)$ that are obtained, respectively, by the following edge-identifications at the same triangle Δ :

$$\tilde{\Gamma}_1 : (E_1E_2E_3) = (E'_3E'_2E'_1), \quad \tilde{\Gamma}_2 : (E_1E_2E_3) = (E'_1E'_3E'_2), \quad \tilde{\Gamma}_3 : (E_1E_2E_3) = (E'_2E'_1E'_3) . \tag{3.9}$$

Note that, in contrast to (3.8), three-dimensional orientation is not preserved across Δ [see Fig. 10(b)]. We introduce a transformation Ω that interchanges two triplets $(\Gamma_1, \Gamma_2, \Gamma_3)$ and $(\tilde{\Gamma}_1, \tilde{\Gamma}_2, \tilde{\Gamma}_3)$, and define *unoriented membrane theories* to be those that are obtained from the oriented theories by the projection operator $(1 + \Omega)/2$ acting on every triangle. We will call the set $(\Gamma_1, \Gamma_2, \Gamma_3, \tilde{\Gamma}_1, \tilde{\Gamma}_2, \tilde{\Gamma}_3)$ the *fundamental sextet associated with triangle* Δ. So far we have assumed that the tetrahedral decomposition Γ_1 is orientable, but one can easily see that Γ_1 is not necessarily orientable for the above definition of a sextet to make sense because we focus only on local configurations around triangle Δ. In the rest of paper, we understand that the domain of definition for Ω is extended so as to include nonorientable tetrahedral decompositions.

Note that each sextet $(\Gamma_1, \ldots, \tilde{\Gamma}_3)$ consists of both manifolds and nonmanifolds, unlike the two-dimensional cases where Ω always relates a manifold to another manifold. In fact, suppose that a tetrahedral decomposition Γ_1 represents a three-dimensional manifold. Then, the change of the edge-identification at Δ from $(E_1E_2E_3) = (E'_1E'_2E'_3)$ to $(E_1E_2E_3) = (E'_3E'_2E'_1)$ gives rise to a singularity at the midpoint of edge $E_2 = E'_2$ in $\tilde{\Gamma}_1$ around which we cannot define a local orientation. The appearance of singularity will be demonstrated explicitly when we consider an example in Sect. 4.3.

4. Triangle–hinge models for unoriented membranes

4.1. Action and Feynman rules

In this section, we realize unoriented membrane theories as triangle–hinge models. We show that they are obtained simply by replacing $C = C_+$ in the original oriented models (2.14) with $C = C_+ + C_-$:

$$\begin{aligned} S &= \frac{1}{2}[AB] - \frac{\lambda}{6}\left([C_+AAA] + [C_-AAA]\right) - \sum_k \frac{\mu_k}{2k}[Y_k \underbrace{B \cdots B}_{k}] \\ &\equiv \frac{1}{2}A_{abcd}B_{abcd} \\ &\quad - \frac{\lambda}{6n^3}\left(\omega^{d_1a_2}\omega^{d_2a_3}\omega^{d_3a_1} + \omega^{d_3a_2}\omega^{d_2a_1}\omega^{d_1a_3}\right)\omega^{b_3c_2}\omega^{b_2c_1}\omega^{b_1c_3}\, A_{a_1b_1c_1d_1}A_{a_2b_2c_2d_2}A_{a_3b_3c_3d_3} \\ &\quad - \sum_k \frac{n^2\mu_k}{2k} B_{a_1a_2b_2b_1}\cdots B_{a_{k-1}a_kb_kb_{k-1}}B_{a_ka_1b_1b_k} . \end{aligned} \tag{4.1}$$

Here, C_+ is again given by Eq. (2.12), and C_- by

$$C_-^{a_1b_1c_1d_1a_2b_2c_2d_2a_3b_3c_3d_3} \equiv \frac{1}{n^3}\,\omega^{d_3a_2}\omega^{d_2a_1}\omega^{d_1a_3}\omega^{b_3c_2}\omega^{b_2c_1}\omega^{b_1c_3} . \tag{4.2}$$

We first note that the interaction vertices corresponding to $[C_+AAA]$ and $[C_-AAA]$ can be expressed by thickened triangles with directed index lines, as in Fig. 11. Contractions using $[C_+AAA]$ yield the identification of a triangle belonging to a tetrahedron with another triangle belonging to an adjacent tetrahedron so that the orientation is preserved [see Fig. 11(a)]. The two positively oriented tetrahedra thus reside in opposite positions with respect to the thickened triangle, and the edges

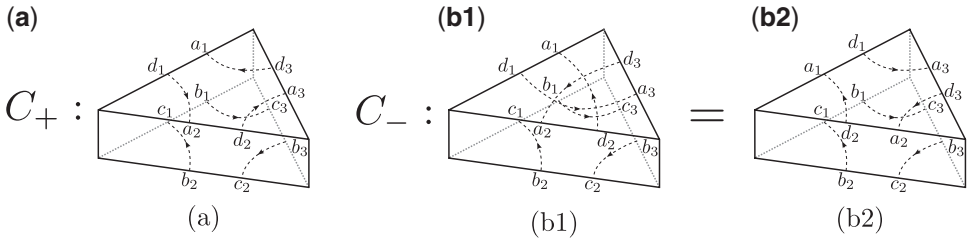

Fig. 11. Interaction vertices corresponding to (a) $[C_+AAA]$ and (b) $[C_-AAA]$. If C_+ represents triangle-identifications which preserve three-dimensional local orientation, C_- represents triangle-identifications which do not preserve orientation.

(a_1, d_1), (a_2, d_2), (a_3, d_3) will be identified with the edges (b_1, c_1), (b_2, c_2), (b_3, c_3), respectively, when we deflate the triangle to get a tetrahedral decomposition. On the contrary, contractions using $[C_-AAA]$ yield an identification of triangles where the orientation is not preserved [see Fig. 11(b1, b2)]. In fact, the indices of C_- [see (4.2)] can be expressed as Fig. 11(b1) or (b2). We use the expression (b1) in a Feynman diagram where the triangle is connected to hinges, but we exploit the other expression (b2) when the thickened triangle is interpreted as representing two triangles to be identified in gluing two tetrahedra of positive orientation. Then, the edges (a_1, d_1), (a_2, d_2), (a_3, d_3) will be identified with the edges (c_1, b_1), (c_2, b_2), (c_3, b_3), respectively, when we deflate triangles to get a tetrahedral decomposition. It is easy to see that the two positively oriented tetrahedra are now in the same position with respect to the triangle and thus will take the configuration of Fig. 8(b1) after the triangle is deflated. This means that the orientation is not preserved for this gluing of tetrahedra.

Note that the direction of arrows on index lines is still preserved for diagrams using C_-. Thus, taking the same large-n limit as in the oriented models, we can reduce the set of diagrams such that all their index polygons are triangles,[14] and can conclude that they represent tetrahedral decompositions.

4.2. Wick contractions corresponding to the fundamental sextet

Recall that for each triangle Δ in a tetrahedral decomposition $\Gamma = \Gamma_1$, we have the fundamental sextet of tetrahedral decompositions, $(\Gamma_1, \Gamma_2, \Gamma_3, \tilde{\Gamma}_1, \tilde{\Gamma}_2, \tilde{\Gamma}_3)$, which close among themselves under the action of Ω. In this subsection, we write down the corresponding sextet $(\gamma_1, \gamma_2, \gamma_3, \tilde{\gamma}_1, \tilde{\gamma}_2, \tilde{\gamma}_3)$ in unoriented triangle–hinge models.

We first note that, while the *total* number of triangles (as well as that of tetrahedra) is the same among the sextet $(\Gamma_1, \ldots, \tilde{\Gamma}_3)$, this is not the case for those numbers around each edge of triangle Δ. For example, let us consider the case where the three edges of Δ in Γ_1 [denoted by $E_1 (= E'_1), E_2 (= E'_2), E_3 (= E'_3)$] are connected to three different hinges. If we change the identification at Δ from $(E_1E_2E_3) = (E'_1E'_2E'_3)$ to $(E_1E_2E_3) = (E'_2E'_3E'_1)$ to obtain Γ_2, all the three edges E_1, E_2, E_3 must be the same due to triangle-identifications at other triangles.[15] Therefore, Feynman diagrams γ_1 and γ_2 in a triangle–hinge model must have different numbers and different types of hinges if they correspond to Γ_1 and Γ_2, respectively. This means that the constructions of sextets are not so straightforward in triangle–hinge models compared to other models (such as tensor models).

[14] As in the original models, a tetrahedron has one index triangle at each corner (see Fig. 6).

[15] Since we assume that Γ is a tetrahedral decomposition without boundaries, other triangle-identifications in Γ ensure the edge-identifications $E_1 = E'_1$, $E_2 = E'_2$, and $E_3 = E'_3$. See the discussions below (4.12) for more details.

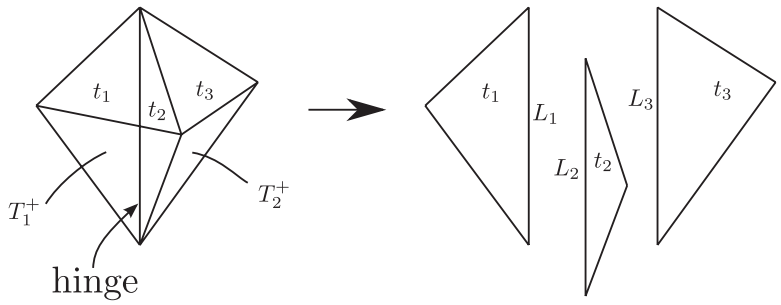

Fig. 12. Labeling of edges around a k-hinge.

Let us take the above consideration to a more concrete form, considering a triangle Δ in a tetrahedral decomposition Γ_1, at which two positively oriented tetrahedra are glued with the orientation being preserved. We first note that there are the following three cases for the three edges I, J, K of triangle Δ:

(1) Three edges I, J, K are connected to three different hinges.

(2) Two and only two of them are connected to the same hinge.

(3) All of them are connected to the same hinge. (4.3)

We suppose that Γ_1 is of the type (1) at Δ, and that edges I, J, K are connected to the $(p+1)$-, $(q+1)$-, $(r+1)$-hinges, respectively. Including p other edges connected to the $(p+1)$-hinge, we label the edges around the $(p+1)$-hinge as $[I, I_1, \ldots, I_p]$ in a cyclic order. Here, we define the cyclic ordering of edges around a k-hinge as follows (see Fig. 12): We first pick up two neighboring triangles t_1 and t_2 belonging to the same tetrahedron T_1^+ of positive orientation, and label their edges connected to the hinge as L_1 and L_2, respectively. Next to T_1^+ there is another positively oriented tetrahedron T_2^+ determined by triangle t_2 and another triangle t_3 sharing the same hinge, and we label as L_3 the edge of t_3 that is connected to the hinge. Repeating this procedure, we obtain a sequence $[L_1, L_2, \ldots, L_k]$ around the k-hinge. Since another choice (t_2, t_3) is possible as the initial pair for the same configuration of edges around the hinge, we should regard the above sequence as being cyclically symmetric, $[L_1, L_2, \ldots, L_k] = [L_2, L_3, \ldots, L_k, L_1]$. Note that, if we take (t_2, t_1) as the initial pair, the edges around the k-hinge will be represented as a sequence in reverse order, $[L_k, \ldots, L_2, L_1]$.

Labeling similarly the edges around the $(q+1)$- and $(r+1)$-hinges by $[J, J_1, \ldots, J_q]$ and $[K, K_1, \ldots, K_r]$, respectively, we have

$$\begin{aligned}\Gamma_1 :\ & \text{edge } I \text{ is connected to a } (p+1)\text{-hinge as } [I, I_1, \ldots, I_p],\\ & \text{edge } J \text{ is connected to a } (q+1)\text{-hinge as } [J, J_1, \ldots, J_q],\\ & \text{edge } K \text{ is connected to a } (r+1)\text{-hinge as } [K, K_1, \ldots, K_r].\end{aligned} \tag{4.4}$$

Then, the remaining tetrahedral decompositions in the sextet have the following configurations:

$$\begin{aligned}\Gamma_2 :\ & \text{three edges } I, J, K \text{ are connected to a single } (p+q+r+3)\text{-hinge}\\ & \text{as } [I, I_1, \ldots, I_p, K, K_1, \ldots, K_r, J, J_1, \ldots, J_q].\end{aligned} \tag{4.5}$$

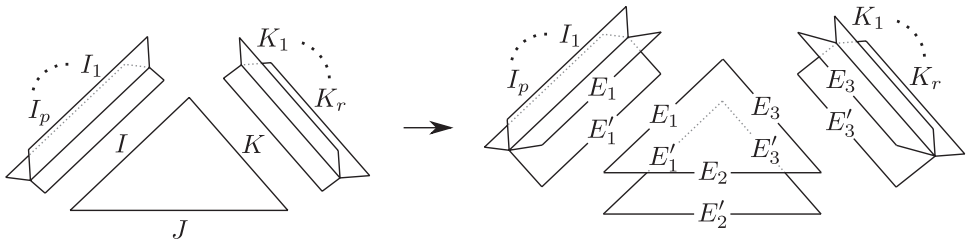

Fig. 13. The splitting of Δ corresponding to Γ_1. Edge I becomes two edges E_1 and E_1', and edge J (or K) becomes E_2 and E_2' (or E_3 and E_3'). The $(p+1)$-, $(q+1)$-, $(r+1)$-hinges accordingly become $(p+2)$-, $(q+2)$-, $(r+2)$-hinges, respectively. Γ_1 is restored by the edge-identification $(E_1E_2E_3) = (E_1'E_2'E_3')$ for the split triangles.

Γ_3 : three edges I, J, K are connected to a single $(p+q+r+3)$-hinge as $[I, I_1, \ldots, I_p, J, J_1, \ldots, J_q, K, K_1, \ldots, K_r]$. (4.6)

$\tilde{\Gamma}_1$: two edges I, K are connected to a $(p+r+2)$-hinge as $[I, I_1, \ldots, I_p, K, K_1, \ldots, K_r]$, and edge J is connected to a $(q+1)$-hinge as $[J, J_1, \ldots, J_q]$. (4.7)

$\tilde{\Gamma}_2$: two edges J, K are connected to a $(q+r+2)$-hinge as $[J, J_1, \ldots, J_q, K, K_1, \ldots, K_r]$, and edge I is connected to a $(p+1)$-hinge as $[I, I_1, \ldots, I_p]$. (4.8)

$\tilde{\Gamma}_3$: two edges I, J are connected to a $(p+q+2)$-hinge as $[I, I_1, \ldots, I_p, J, J_1, \ldots, J_q]$, and edge K is connected to a $(r+1)$-hinge as $[K, K_1, \ldots, K_r]$. (4.9)

Equations (4.4)–(4.9) can be understood in the following way. We begin with (4.4), which is the simplest and most obvious. We first split the triangle Δ in Γ_1 into two triangles as in Fig. 13 in order to realize the configuration before the edge-identification $(E_1E_2E_3) = (E_1'E_2'E_3')$ is made. This splitting is accompanied by that of edge I to two edges E_1 and E_1', and that of edge J (or K) to E_2 and E_2' (or to E_3 and E_3'). Accordingly, the $(p+1)$-, $(q+1)$-, $(r+1)$-hinges are transformed to $(p+2)$-, $(q+2)$-, $(r+2)$-hinges, respectively. Now we follow the sequence of the edges connected to each hinge in the other direction. If we start from the edge E_1 connected to the $(p+2)$-hinge, we then pass through the edges $I_1, \ldots, I_p$ following the original sequence $[I, I_1, \ldots, I_p]$, and reach the edge E_1', which will be identified with the starting edge E_1 (i.e., $E_1' = E_1 = I$) under the edge-identification for Γ_1, $(E_1E_2E_3) = (E_1'E_2'E_3')$. Let us write the total path schematically as a cycle,

$$\bullet\, E_1 \to I_1 \to \cdots \to I_p \to E_1' = E_1. \tag{4.10}$$

Similarly, if we start from the edge E_2 connected to the $(q+2)$-hinge or from the edge E_3 connected to the $(r+2)$-hinge, we then have the following paths:

$$\bullet\, E_2 \to J_1 \to \cdots \to J_q \to E_2' = E_2, \tag{4.11}$$

$$\bullet\, E_3 \to K_1 \to \cdots \to K_r \to E_3' = E_3. \tag{4.12}$$

Equations (4.10)–(4.12) are exactly what is expressed in (4.4).

Now we consider the tetrahedral decomposition Γ_2, which was obtained from Γ_1 by changing the edge-identification from $(E_1E_2E_3) = (E_1'E_2'E_3')$ to $(E_1E_2E_3) = (E_2'E_3'E_1')$ [see Fig. 14(a)]. If we start from the edge E_1 connected to the $(p+2)$-hinge, we then again pass through the edges $I_1, \ldots, I_p$ and reach the edge E_1'. However, this is not the end of the journey because E_1' will be identified with

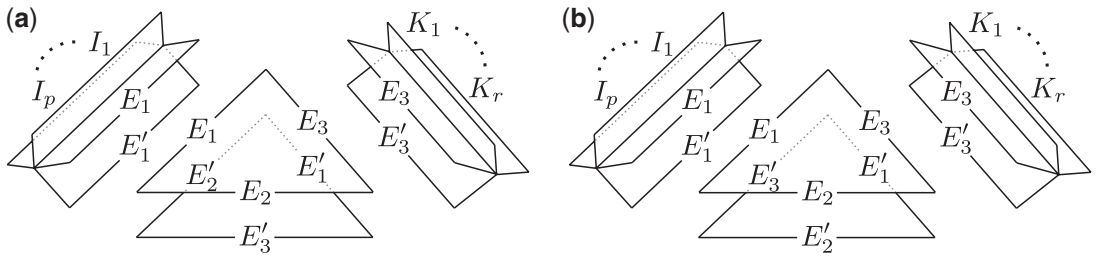

Fig. 14. The splittings of Δ corresponding to (a) Γ_2 and (b) $\tilde{\Gamma}_1$. Γ_2 is obtained by the edge-identification $(E_1E_2E_3) = (E_2'E_3'E_1')$ for the split triangles, and $\tilde{\Gamma}_1$ by $(E_1E_2E_3) = (E_3'E_2'E_1')$ for the split triangles.

E_3 in the edge-identification, and we need to follow another sequence of edges, $K_1, \ldots, K_r$, to reach E_3'. Since E_3' will be identified with E_2, we need to continue the journey; we pass through the edges $J_1, \ldots, J_q$ to reach E_2', which finally will agree with the starting edge E_1. The total path can thus be written as the following cycle:

$$\begin{aligned} &\bullet\, E_1 \to I_1 \to \cdots \to I_p \to E_1' = E_3 \to K_1 \to \cdots \to K_r \\ &\quad \to E_3' = E_2 \to J_1 \to \cdots \to J_q \to E_2' = E_1. \end{aligned} \tag{4.13}$$

Since $E_1' = E_3 = K$, $E_3' = E_2 = J$, and $E_2' = E_1 = I$ under the edge-identification, the path (4.13) can be written as (4.5). Similarly, (4.6) can be understood from the path:

$$\begin{aligned} &\bullet\, E_1 \to I_1 \to \cdots \to I_p \to E_1' = E_2 \to J_1 \to \cdots \to J_q \\ &\quad \to E_2' = E_3 \to K_1 \to \cdots \to K_r \to E_3' = E_1. \end{aligned} \tag{4.14}$$

Equation (4.7) can be understood in a similar way, by recalling that $\tilde{\Gamma}_1$ is obtained from Γ_1 by changing the edge-identification from $(E_1E_2E_3) = (E_1'E_2'E_3')$ to $(E_1E_2E_3) = (E_3'E_2'E_1')$ [see Fig. 14(b)], which gives the following two disconnected cycles:

$$\begin{aligned} &\bullet\, E_1 \to I_1 \to \cdots \to I_p \to E_1' = E_3 \to K_1 \to \cdots \to K_r \to E_3' = E_1, \\ &\bullet\, E_2 \to J_1 \to \cdots \to J_q \to E_2' = E_2. \end{aligned} \tag{4.15}$$

Similarly, the cycles for $\tilde{\Gamma}_2$ [edge-identification $(E_1E_2E_3) = (E_1'E_3'E_2')$] are given by

$$\begin{aligned} &\bullet\, E_2 \to J_1 \to \cdots \to J_q \to E_2' = E_3 \to K_1 \to \cdots \to K_r \to E_3' = E_2, \\ &\bullet\, E_1 \to I_1 \to \cdots \to I_p \to E_1' = E_1, \end{aligned} \tag{4.16}$$

and those for $\tilde{\Gamma}_3$ [edge-identification $(E_1E_2E_3) = (E_2'E_1'E_3')$] are given by

$$\begin{aligned} &\bullet\, E_1 \to I_1 \to \cdots \to I_p \to E_1' = E_2 \to J_1 \to \cdots \to J_q \to E_2' = E_1, \\ &\bullet\, E_3 \to K_1 \to \cdots \to K_r \to E_3' = E_3. \end{aligned} \tag{4.17}$$

Now that we understand in detail the configurations of the fundamental sextet $(\Gamma_1, \ldots, \tilde{\Gamma}_3)$ associated with triangle Δ, it is easy to translate (4.4)–(4.9) in terms of unoriented triangle–hinge models, and we obtain the sextet of Feynman diagrams $(\gamma_1, \ldots, \tilde{\gamma}_3)$ as the following groups of

Wick contractions:[16]

$$\gamma_1: \quad [C_+A_IA_JA_K]X_{I_1\ldots I_p,J_1\ldots J_q,K_1\ldots K_r} \times [Y_{p+1}B_I^{(+)}B_{I_1}^{\sigma_{I_1}}\cdots B_{I_p}^{\sigma_{I_p}}][Y_{q+1}B_J^{(+)}B_{J_1}^{\sigma_{J_1}}\cdots B_{J_q}^{\sigma_{J_q}}][Y_{r+1}B_K^{(+)}B_{K_1}^{\sigma_{K_1}}\cdots B_{K_r}^{\sigma_{K_r}}], \tag{4.18}$$

$$\gamma_2: \quad [C_+A_IA_JA_K]X_{I_1\ldots I_p,J_1\ldots J_q,K_1\ldots K_r} \times [Y_{p+q+r+3}B_I^{(+)}B_{I_1}^{\sigma_{I_1}}\cdots B_{I_p}^{\sigma_{I_p}}B_K^{(+)}B_{K_1}^{\sigma_{K_1}}\cdots B_{K_r}^{\sigma_{K_r}}B_J^{(+)}B_{J_1}^{\sigma_{J_1}}\cdots B_{J_q}^{\sigma_{J_q}}], \tag{4.19}$$

$$\gamma_3: \quad [C_+A_IA_JA_K]X_{I_1\ldots I_p,J_1\ldots J_q,K_1\ldots K_r} \times [Y_{p+q+r+3}B_I^{(+)}B_{I_1}^{\sigma_{I_1}}\cdots B_{I_p}^{\sigma_{I_p}}B_J^{(+)}B_{J_1}^{\sigma_{J_1}}\cdots B_{J_q}^{\sigma_{J_q}}B_K^{(+)}B_{K_1}^{\sigma_{K_1}}\cdots B_{K_r}^{\sigma_{K_r}}], \tag{4.20}$$

$$\tilde{\gamma}_1: \quad [C_-A_IA_JA_K]X_{I_1\ldots I_p,J_1\ldots J_q,K_1\ldots K_r} \times [Y_{p+r+2}B_I^{(+)}B_{I_1}^{\sigma_{I_1}}\cdots B_{I_p}^{\sigma_{I_p}}B_K^{(+)}B_{K_1}^{\sigma_{K_1}}\cdots B_{K_r}^{\sigma_{K_r}}][Y_{q+1}B_J^{(+)}B_{J_1}^{\sigma_{J_1}}\cdots B_{J_q}^{\sigma_{J_q}}], \tag{4.21}$$

$$\tilde{\gamma}_2: \quad [C_-A_IA_JA_K]X_{I_1\ldots I_p,J_1\ldots J_q,K_1\ldots K_r} \times [Y_{q+r+2}B_J^{(+)}B_{J_1}^{\sigma_{J_1}}\cdots B_{J_q}^{\sigma_{J_q}}B_K^{(+)}B_{K_1}^{\sigma_{K_1}}\cdots B_{K_r}^{\sigma_{K_r}}][Y_{p+1}B_I^{(+)}B_{I_1}^{\sigma_{I_1}}\cdots B_{I_p}^{\sigma_{I_p}}], \tag{4.22}$$

$$\tilde{\gamma}_3: \quad [C_-A_IA_JA_K]X_{I_1\ldots I_p,J_1\ldots J_q,K_1\ldots K_r} \times [Y_{p+q+2}B_I^{(+)}B_{I_1}^{\sigma_{I_1}}\cdots B_{I_p}^{\sigma_{I_p}}B_J^{(+)}B_{J_1}^{\sigma_{J_1}}\cdots B_{J_q}^{\sigma_{J_q}}][Y_{r+1}B_K^{(+)}B_{K_1}^{\sigma_{K_1}}\cdots B_{K_r}^{\sigma_{K_r}}]. \tag{4.23}$$

Here, we have used the abbreviation for Wick contractions introduced in Sect. 2.1, and the superscript σ takes $(+)$ or $(-)$. We have written explicitly only for the part of the interaction vertices corresponding to Δ (expressed by $[C_\pm A_IA_JA_K]$) and the hinges connected to Δ. The remaining part (denoted by $X_{I_1\ldots I_p,J_1\ldots J_q,K_1\ldots K_r}$) is common among the sextet $(\gamma_1,\ldots,\tilde{\gamma}_3)$ and represents the other interaction vertices and their contractions.[17] As for diagrams $\gamma_1,\gamma_2,\gamma_3$, the identification at Δ preserves the orientation as in Fig. 10(a), and thus we have used the vertex $[C_+A_IA_JA_K]$. On the other hand, as for diagrams $\tilde{\gamma}_1,\tilde{\gamma}_2,\tilde{\gamma}_3$, the identification at Δ does not preserve the orientation as in Fig. 10(b), and thus we have used the vertex $[C_-A_IA_JA_K]$. In Appendix A we prove that the diagrams $\gamma_2,\ldots,\tilde{\gamma}_3$ represent tetrahedral decompositions if γ_1 does.

So far we have assumed that the orientation is preserved at Δ in Γ_1 and also that Γ_1 is of type (1) in (4.3). For other cases, one can also obtain the corresponding sextets $(\gamma_1,\ldots,\tilde{\gamma}_3)$ in a similar way.

4.3. Example

To understand the meaning of the above sextet (4.18)–(4.23), let us consider a simple example. We take a tetrahedral decomposition Γ_1 of a three-sphere, consisting of two tetrahedra glued together at their faces as shown in Fig. 15. Diagram γ_1 representing Γ_1 is realized by the following group of Wick contractions [Eq. (4.18)]:

$$[C_+A_IA_JA_K]_\Delta[Y_2B_I^{(+)}B_{I_1}^{(-)}][Y_2B_J^{(+)}B_{J_1}^{(-)}][Y_2B_K^{(+)}B_{K_1}^{(-)}] \times X_{I_1J_1K_1}, \tag{4.24}$$

$$X_{I_1J_1K_1} = [C_+A_{I_1}A_{M_1}A_{N_2}]_1[C_+A_{J_1}A_{N_1}A_{L_2}]_2[C_+A_{K_1}A_{L_1}A_{M_2}]_3 \times [Y_2B_{L_1}^{(+)}B_{L_2}^{(-)}][Y_2B_{M_1}^{(+)}B_{M_2}^{(-)}][Y_2B_{N_1}^{(+)}B_{N_2}^{(-)}]. \tag{4.25}$$

[16] Due to the cyclic symmetry of C_+, a group of Wick contractions containing $[C_+A_IA_JA_K]$ and that containing $[C_+A_JA_KA_I]$ represent the same Feynman diagram.

[17] $X_{I_1\ldots K_r}$ includes $A_{I_1},\ldots,A_{K_r}$, which are the partners of $B_{I_1},\ldots,B_{K_r}$ in the Wick contractions.

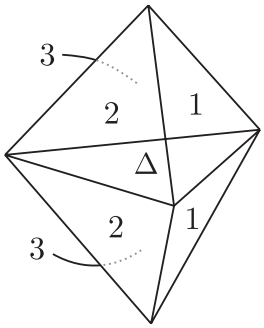

Fig. 15. Tetrahedral decomposition Γ_1 of three-sphere, where triangles with the same label are identified.

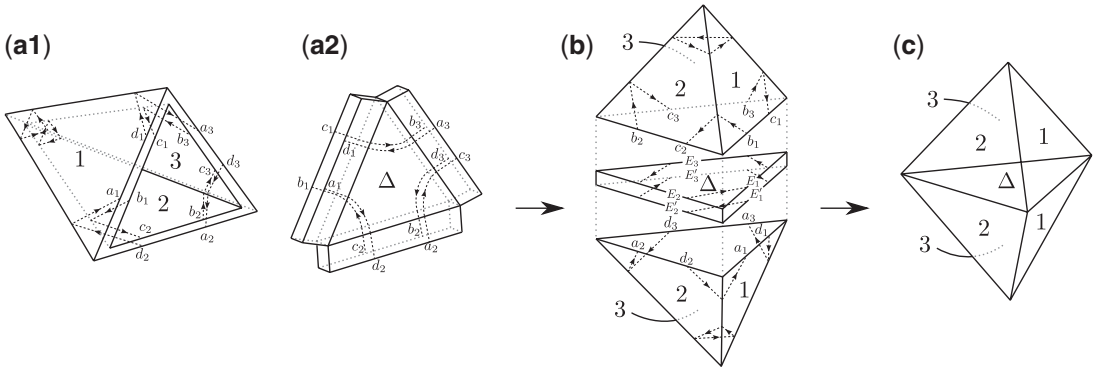

Fig. 16. Feynman diagram γ_1 representing Γ_1. (a1) The part corresponding to X. (a2) The part corresponding to Δ. The interaction vertices corresponding to triangles are specified by the labels $\Delta, 1, 2, 3$. Three 2-hinges exist in (a1) but are not displayed explicitly there. (b) Edge-identification at Δ, which is realized by contracting (a1) and (a2). (c) The obtained tetrahedral decomposition Γ_1.

Here, the subscripts $\Delta, 1, 2, 3$ specify the triangles corresponding to the interaction vertices; Δ specifies the triangle at which we change the edge-identification to obtain $\gamma_2, \ldots, \tilde{\gamma}_3$, and $1, 2, 3$ specify the triangles belonging to the remaining part X, which consists of three triangles $(1, 2, 3)$ and three 2-hinges (see Fig. 16). Figure 16(a1) depicts the part corresponding to X, while Fig. 16(a2) depicts the part corresponding to Δ, which consists of a triangle and three 2-hinges. In Fig. 16(a1) and (a2), edges with the same indices are connected by contractions. Recalling that the edge-identification of Γ_1 is expressed by $(E_1E_2E_3) = (E'_1E'_2E'_3)$, we label the ordered indices (b_i, c_i) and (a_i, d_i) $(i = 1, 2, 3)$ in Fig. 16(a1) as $E_i = E_i(b_i, c_i)$ and $E'_i = E'_i(a_i, d_i)$, respectively. Since edges E_i and E'_i are expressed as in Fig. 16(b) when (a1) and (a2) are combined, we see that the edge-identification $(E_1E_2E_3) = (E'_1E'_2E'_3)$ will certainly be realized after triangle Δ is deflated.

Now we consider diagram γ_2 representing the tetrahedral decomposition Γ_2 that is obtained from Γ_1 by changing the edge-identification from $(E_1E_2E_3) = (E'_1E'_2E'_3)$ to $(E_1E_2E_3) = (E'_2E'_3E'_1)$ (see Fig. 17). Note that Γ_2 has the topology of a three-dimensional lens space $L(3, 1)$, as can be seen from Fig. 17(c). Diagram γ_2 is given by (4.19), that is,

$$[C_+A_IA_JA_K][Y_6B_I^{(+)}B_{I_1}^{(-)}B_K^{(+)}B_{K_1}^{(-)}B_J^{(+)}B_{J_1}^{(-)}] \times X_{I_1J_1K_1} \,. \tag{4.26}$$

Since the part given by X is common among the sextet, we have the same labeling of edges, $E_i(b_i, c_i)$ and $E'_i(a_i, d_i)$ $(i = 1, 2, 3)$, and diagram γ_2 takes the form shown in Fig. 17(a1) and (a2). In Fig. 17(a2), the ordered indices (b_1, c_1) are connected to (g, f) by index lines, and (a_2, d_2)

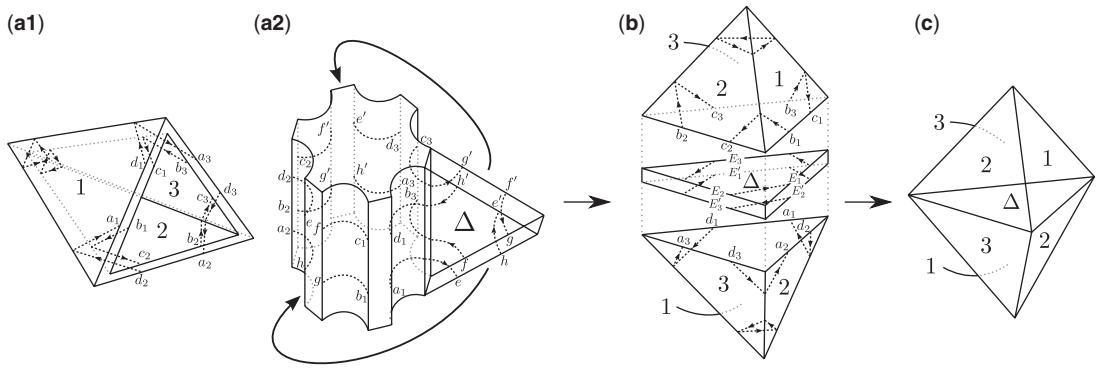

Fig. 17. Feynman diagram γ_2 representing Γ_2. (a1) The part corresponding to X. (a2) The part corresponding to Δ. (b) The edge-identification at Δ. (c) The obtained tetrahedral decomposition Γ_2.

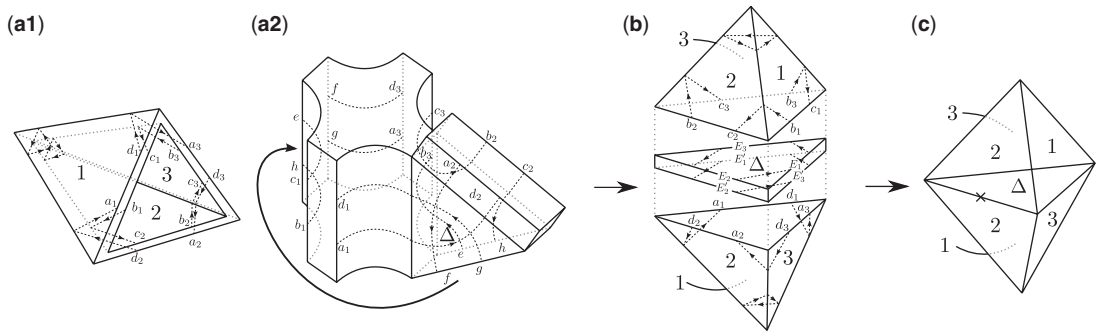

Fig. 18. Feynman diagram $\tilde{\gamma}_1$ representing $\tilde{\Gamma}_1$. (a1) The part corresponding to X. (a2) The part corresponding to Δ. (b) The edge-identification at Δ. (c) The obtained tetrahedral decomposition $\tilde{\Gamma}_1$, where the midpoint of the edge shared by triangles 2 and Δ is singular.

are connected to (h,e). Thus, as can be seen from Fig. 17(b), edge $E_1(b_1,c_1) = (g,f)$ will be identified with edge $E_2'(a_2,d_2) = (h,e)$ after triangle Δ is deflated. Similarly, edges $E_2(b_2,c_2)$ and $E_3(b_3,c_3)$ will be identified with edges $E_3'(a_3,d_3)$ and $E_1'(a_1,d_1)$, respectively. We thus obtain the edge-identification $(E_1E_2E_3) = (E_2'E_3'E_1')$ of Γ_2. In a similar way, we can realize Γ_3 [resulting from the edge-identification $(E_1E_2E_3) = (E_3'E_1'E_2')$ at Δ] as a diagram γ_3 [Eq. (4.20)] of a triangle–hinge model. Γ_3 has the topology of a lens space $L(3,2) = L(3,1)$. Thus, in this simple example, two diagrams γ_2 and γ_3 represent the same tetrahedral decomposition, $\Gamma_2 = \Gamma_3$.

As for the tetrahedral decomposition $\tilde{\Gamma}_1$ [resulting from the edge-identification $(E_1E_2E_3) = (E_3'E_2'E_1')$ at Δ], the corresponding diagram $\tilde{\gamma}_1$ is obtained from the following group of Wick contractions [Eq. (4.21)]:

$$[C_-A_IA_JA_K][Y_4B_I^{(+)}B_{I_1}^{(-)}B_K^{(+)}B_{K_1}^{(-)}][Y_2B_J^{(+)}B_{J_1}^{(-)}] \times X_{I_1J_1K_1}\,. \tag{4.27}$$

The diagram is depicted in Fig. 18. In Fig. 18(a2), the ordered indices (b_1,c_1) are connected to (h,e) by index lines, and (d_3,a_3) are connected to (f,g). Thus, due to the edge-identification for C_- explained below (4.2), edge $E_1(b_1,c_1) = (h,e)$ will be identified with edge $E_3'(d_3,a_3) = (f,g)$ after triangle Δ is deflated. Similarly, edges $E_2(b_2,c_2)$ and $E_3(b_3,c_3)$ will be identified with edges $E_2'(d_2,a_2)$ and $E_1'(d_1,a_1)$, respectively. We thus obtain the edge-identification $(E_1E_2E_3) = (E_3'E_2'E_1')$ of $\tilde{\Gamma}_1$. Although $\tilde{\Gamma}_1$ consists of two tetrahedra, it is not a three-dimensional manifold. In fact, there is a singularity at the midpoint of edge $E_2 = E_2'$ of Δ, around which we cannot define a local orientation.

It is easy to see that the other diagrams $\tilde{\gamma}_2$ and $\tilde{\gamma}_3$ are realized by (4.22) and (4.23), respectively, and represent the same tetrahedral decomposition as $\tilde{\Gamma}_1$.

4.4. Note on the weights of diagrams

We comment that a sextet $(\gamma_1, \gamma_2, \gamma_3, \tilde{\gamma}_1, \tilde{\gamma}_2, \tilde{\gamma}_3)$ appears in the free energy with the same coefficients. By "the same coefficients" we mean that the numerical factors of these diagrams are the same except for powers of n, λ, μ_k if we treat the common part X as a set of distinguished external vertices and sum over all diagrams representing the same tetrahedral decomposition.

We note that, if a group x of Wick contractions represents a tetrahedral decomposition and if all the interaction vertices are distinguished, then x contributes to the free energy as[18]

$$\frac{1}{s_2!}\left(\frac{\lambda}{6n}\right)^{s_2}\prod_{k=1}\left[\frac{1}{s_1^k!}\left(\frac{n^2\mu_k}{2k}\right)^{s_1^k}\right]. \tag{4.28}$$

Here, s_2 and s_1^k denote the numbers of triangles and k-hinges, respectively, in diagram $\gamma = [x]$. Thus, there arise $1/(s_2!\,6^{s_2})$ and $1/(s_1^k!\,(2k)^{s_1^k})$ in the free energy as numerical factors.

If there are n_k internal k-hinges in a diagram,[19] there are $n_k!$ different contractions corresponding to the permutation of these hinges, since the external vertices are distinguished. For each k-hinge, there are $2k$ ways to give the same diagram due to the symmetry of k-hinge vertices. Thus, the numerical factor of each contraction, $1/(n_k!(2k)^{n_k})$, is compensated if we sum these contributions. The numerical factor $1/6$ of triangle Δ is also canceled. Actually, since C_+ has the symmetry (2.13) there are six ways to give the same diagram. The above computation ensures that three diagrams $\gamma_1, \gamma_2, \gamma_3$ are generated with unit coefficient in the original triangle–hinge model. Furthermore, since C_- also has the symmetry

$$C_-^{i_1j_1i_2j_2i_3j_3} = C_-^{i_2j_2i_3j_3i_1j_1} = C_-^{j_1i_1j_2i_2j_3i_3}, \tag{4.29}$$

$\tilde{\gamma}_1, \tilde{\gamma}_2, \tilde{\gamma}_3$ are also generated with unit coefficient in an unoriented model.

5. Matter fields in unoriented triangle–hinge models

In this section we show that matter fields can be introduced to unoriented triangle–hinge models in the same way as the original triangle–hinge models [2]. We focus here on assigning matter degrees of freedom only to tetrahedra, but the assignment can be done to simplices of any dimensions, as in [2].

Introducing matter degrees of freedom is realized by coloring each tetrahedron in tetrahedral decompositions. Actually, we only need to repeat the steps given in [2]. We first extend the algebra $\mathcal{A}$ to a tensor product of the form $\mathcal{A} = \mathcal{A}_{\text{grav}} \otimes \mathcal{A}_{\text{mat}}$. Here, $\mathcal{A}_{\text{grav}}$ is again $M_{n=3m}(\mathbb{R})$, and we take $\mathcal{A}_{\text{mat}}$ to be $M_{|\mathcal{J}|}(\mathbb{R})$, where $\mathcal{J}$ is the set of colors. Now the dynamical variables A, B have eight indices $A = (A_{ab\alpha\beta,cd\gamma\delta})$, $B = (B_{ab\alpha\beta,cd\gamma\delta})$, where the indices a, b, c, d correspond to $\mathcal{A}_{\text{grav}}$, and $\alpha, \beta, \gamma, \delta$ to $\mathcal{A}_{\text{mat}}$.[20] Next we set the tensor C to take the form $C = C_+ + C_-$ ($C_\pm$ represents two ways to

[18] The n dependence comes from the assumption that all the index polygons are triangles.

[19] Internal hinges mean the parts not in X but connected to Δ.

[20] A and B are real-valued matrices symmetric with respect to the pair of indices, $A_{ab\alpha\beta,cd\gamma\delta} = A_{cd\gamma\delta,ab\alpha\beta}$, $B_{ab\alpha\beta,cd\gamma\delta} = B_{cd\gamma\delta,ab\alpha\beta}$.

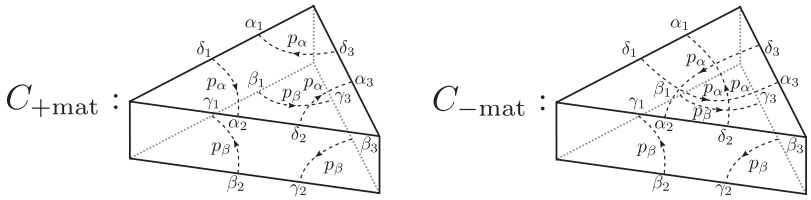

Fig. 19. Interaction vertices corresponding to a triangle ($\mathcal{A}_{\mathrm{mat}}$ part). The upper (lower) side of each triangle has color α (β).

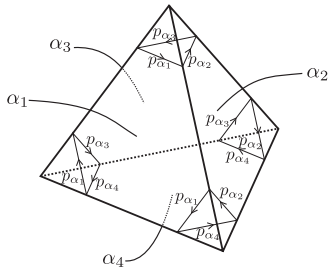

Fig. 20. Index triangles inside a tetrahedron with triangles colored as in (5.1), (5.2) [2].

glue tetrahedra depicted in Fig. 11), and assume that each has a factorized form $C_{\pm} = C_{\pm\mathrm{grav}} C_{\pm\mathrm{mat}}$. Here, we set $C_{\pm\mathrm{grav}}$ to the form (4.1), and let $C_{\pm\mathrm{mat}}$ take the following form:

$$C_{+\mathrm{mat}}^{\alpha_1\beta_1\gamma_1\delta_1\alpha_2\beta_2\gamma_2\delta_2\alpha_3\beta_3\gamma_3\delta_3} = \sum_{\alpha,\beta\in\mathcal{J}} \lambda_{\alpha\beta}\, p_\alpha^{\delta_1\alpha_2} p_\alpha^{\delta_2\alpha_3} p_\alpha^{\delta_3\alpha_1} p_\beta^{\beta_3\gamma_2} p_\beta^{\beta_2\gamma_1} p_\beta^{\beta_1\gamma_3}\,, \tag{5.1}$$

$$C_{-\mathrm{mat}}^{\alpha_1\beta_1\gamma_1\delta_1\alpha_2\beta_2\gamma_2\delta_2\alpha_3\beta_3\gamma_3\delta_3} = \sum_{\alpha,\beta\in\mathcal{J}} \lambda_{\alpha\beta}\, p_\alpha^{\delta_3\alpha_2} p_\alpha^{\delta_2\alpha_1} p_\alpha^{\delta_1\alpha_3} p_\beta^{\beta_3\gamma_2} p_\beta^{\beta_2\gamma_1} p_\beta^{\beta_1\gamma_3}\,, \tag{5.2}$$

where $p_\alpha = (p_\alpha^{\beta\gamma} = \delta_\alpha^\beta \delta_\alpha^\gamma)$ is the projector to the αth component and $\lambda_{\alpha\beta}$ is a real constant. Equations (5.1) and (5.2) mean that we insert p_α to each of the index lines (as ω was inserted for $\mathcal{A}_{\mathrm{grav}}$) and take a summation over α and β with weight $\lambda_{\alpha\beta}$. The $\mathcal{A}_{\mathrm{mat}}$ part of the interaction vertex $[C_+A^3] + [C_-A^3]$ can be illustrated as in Fig. 19. Note that p_α is common among three index lines on each side of a triangle. Thus, one can say that each side of a triangle has a color.

In this construction, the index function $\mathcal{F}(\gamma)$ of diagram γ is factorized to the form

$$\mathcal{F}(\gamma) \equiv \mathcal{F}(\gamma;\mathcal{A}) = \mathcal{F}(\gamma;\mathcal{A}_{\mathrm{grav}})\mathcal{F}(\gamma;\mathcal{A}_{\mathrm{mat}}) \equiv \mathcal{F}_{\mathrm{grav}}(\gamma)\mathcal{F}_{\mathrm{mat}}(\gamma), \tag{5.3}$$

and the factor $\mathcal{F}_{\mathrm{grav}}(\gamma)$ ensures that diagram γ represents a tetrahedral decomposition. The index lines corresponding to $\mathcal{A}_{\mathrm{mat}}$ also form index triangles (see Fig. 20). A tetrahedron surrounded by four sides of triangles with color $\alpha_1, \alpha_2, \alpha_3, \alpha_4$ gives the factor

$$\begin{aligned} &\mathrm{tr}(p_{\alpha_1}p_{\alpha_2}p_{\alpha_3})\mathrm{tr}(p_{\alpha_2}p_{\alpha_1}p_{\alpha_4})\mathrm{tr}(p_{\alpha_1}p_{\alpha_3}p_{\alpha_4})\mathrm{tr}(p_{\alpha_3}p_{\alpha_2}p_{\alpha_4}) \\ &= \begin{cases} 1 & (\alpha_1 = \alpha_2 = \alpha_3 = \alpha_4) \\ 0 & (\text{otherwise}). \end{cases} \end{aligned} \tag{5.4}$$

This means that $\mathcal{F}_{\mathrm{mat}}(\gamma)$ can take nonvanishing values only when four sides of triangles of each tetrahedron have the same color (say α), which enables us to say that the tetrahedron has the color α. We thus succeed in coloring tetrahedra in γ.

If two tetrahedra with color α and β are glued at their faces, the face (corresponding to $C_{\pm\mathrm{mat}}$) gives the factor $\lambda_{\alpha\beta}$. In this sense the coupling constants $\lambda_{\alpha\beta}$ define a local interaction between the color α and β [2]. If we take the set of colors, $\mathcal{J}$, to be $\mathbb{R}^D = \{\mathbf{x}\}$ and let the coupling constants $\lambda_{\mathbf{x},\mathbf{y}}$ ($\mathbf{x}, \mathbf{y} \in \mathbb{R}^D$) take nonvanishing values only around $\mathbf{y}$ as a function of $\mathbf{x}$, then $\mathbf{x}$ can be interpreted as the target space coordinates of a tetrahedron in $\mathbb{R}^D$. Since neighboring tetrahedra are locally connected in $\mathbb{R}^D$, the model can describe the dynamics of unoriented membranes embedded in $\mathbb{R}^D$.

6. Conclusion and outlook

In this paper, we first defined unoriented membrane theories in terms of tetrahedral decompositions, and then realized them as triangle–hinge models. Unoriented membrane theories are obtained from oriented open membrane theories of disk topology by gauging the worldvolume parity transformation Ω. For each triangle Δ in a tetrahedral decomposition, we have introduced two types of triplets, $(\Gamma_1, \Gamma_2, \Gamma_3)$ and $(\tilde{\Gamma}_1, \tilde{\Gamma}_2, \tilde{\Gamma}_3)$, which respectively correspond to two ways of identification at Δ, (3.8) and (3.9). The transformation Ω is then defined as the interchange between $(\Gamma_1, \Gamma_2, \Gamma_3)$ and $(\tilde{\Gamma}_1, \tilde{\Gamma}_2, \tilde{\Gamma}_3)$. After gauging Ω, an unoriented membrane theory treats all the tetrahedral decompositions in the sextet $(\Gamma_1, \Gamma_2, \Gamma_3, \tilde{\Gamma}_1, \tilde{\Gamma}_2, \tilde{\Gamma}_3)$ equally.

An unoriented membrane theory is realized as a triangle–hinge model with the action (4.1). It generates Feynman diagrams representing unoriented tetrahedral decompositions. We gave explicitly in (4.18)–(4.23) the sextet of Feynman diagrams $(\gamma_1, \ldots, \tilde{\gamma}_3)$ corresponding to $(\Gamma_1, \ldots, \tilde{\Gamma}_3)$, and showed that these six diagrams appear with unit coefficient up to factors of coupling constants if we treat the common part X as a set of distinguished external vertices and sum over all Wick contractions giving the same diagram. We further showed that matter degrees of freedom can be introduced to unoriented triangle–hinge models by coloring tetrahedra as carried out in [2]. Although we only discussed the coloring of tetrahedra in this paper, we can set matter degrees of freedom to simplices of any dimensions (i.e. tetrahedra, triangles, edges, and/or vertices) as in [2].

We expect that unoriented triangle–hinge models are solvable at least at the same level as the original oriented models (M. Fukuma, S. Sugishita, and N. Umeda, in preparation), since the dynamical variables are the same type of matrices and the actions have almost the same structure as the original oriented triangle–hinge models. The unoriented models actually might be easier to solve than the original oriented models, because the interaction term corresponding to a triangle has higher symmetry, which may help us to carry out the path integrals more analytically. It is interesting to study critical behaviors of the models in both analytical and numerical ways.

Acknowledgments

The authors thank Naoki Sasakura for useful discussions. MF is supported by MEXT (Grant No. 23540304). SS is supported by the JSPS fellowship.

Funding

Open Access funding: SCOAP[3].

Appendix A. Sextet as tetrahedral decompositions

In this Appendix, we show that the diagrams $\gamma_2, \ldots, \tilde{\gamma}_3$ represent tetrahedral decompositions if γ_1 does. Let us look into the indices in the group of Wick contractions (4.18). We label the indices of B_{I_1} as $B_{a'_{I_1} b'_{I_1} c'_{I_1} d'_{I_1}}$, while we label those of A_{I_1} as $A_{a_{I_1} b_{I_1} c_{I_1} d_{I_1}}$ or $A_{c_{I_1} d_{I_1} a_{I_1} b_{I_1}}$ according to $\sigma_{I_1} = (+)$

or $(-)$, so that we always have

$$\overbrace{A_{I_1}B_{I_1}}^{\sigma_{I_1}} = \delta_{a_{I_1}a'_{I_1}}\delta_{b_{I_1}b'_{I_1}}\delta_{c_{I_1}c'_{I_1}}\delta_{d_{I_1}d'_{I_1}}. \tag{A.1}$$

We use a similar labeling for other A_{I_i} and B_{I_i}. Through the parts other than X in (4.18), indices a_{I_1}, …, d_{K_r} of X are connected to each other by index lines. The other parts are given by

$$[C_+A_IA_JA_K] = A_{a_Ib_Ic_Id_I}A_{a_Jb_Jc_Jd_J}A_{a_Kb_Kc_Kd_K}\omega^{d_Ia_J}\omega^{d_Ja_K}\omega^{d_Ka_I}\omega^{b_Kc_J}\omega^{b_Jc_I}\omega^{b_Ic_K}, \tag{A.2}$$

$$[Y_{p+1}B_IB_{I_1}\cdots B_{I_p}] = B_{a'_Ib'_Ic'_Id'_I}B_{a'_{I_1}b'_{I_1}c'_{I_1}d'_{I_1}}\cdots B_{a'_{I_p}b'_{I_p}c'_{I_p}d'_{I_p}}\delta_{b'_Ia'_{I_1}}\cdots\delta_{b'_{I_p}a'_I}\delta_{c'_Id'_{I_1}}\cdots\delta_{c'_{I_p}d'_I}. \tag{A.3}$$

Thus, by combining them with (A.1), the index lines connecting a_{I_1}, …, d_{K_r} are given by

$$\omega^{c_{I_p}b_{J_q}}\omega^{c_{J_q}b_{K_r}}\omega^{c_{K_r}b_{I_p}}\omega^{a_{K_1}d_{J_1}}\omega^{a_{J_1}d_{I_1}}\omega^{a_{I_1}d_{K_1}}\delta_{b_{I_1}a_{I_2}}\cdots\delta_{b_{I_{p-1}}a_{I_p}}\delta_{c_{I_1}d_{I_2}}\cdots\delta_{c_{I_{p-1}}d_{I_p}}\cdots. \tag{A.4}$$

One can find that index lines out of X take the same form as (A.4) in diagrams γ_2, …, $\tilde{\gamma}_3$. Since we assume that diagram γ_1 represents tetrahedral decomposition Γ_1, all the index loops in γ_1 make index triangles. Then, the index loops of γ_2, …, $\tilde{\gamma}_3$ also must make only index triangles because the index loops have the same form as those of γ_1. We thus have shown that the diagrams represent tetrahedral decompositions if γ_1 does.

References

[1] M. Fukuma, S. Sugishita, and N. Umeda, J. High Energy Phys. **1507**, 088 (2015) [arXiv:1503.08812 [hep-th]] [Search INSPIRE].
[2] M. Fukuma, S. Sugishita, and N. Umeda, arXiv:1504.03532 [hep-th] [Search INSPIRE] to appear in Prog. Theor. Phys.
[3] R. Gurau, Commun. Math. Phys. **304**, 69 (2011) [arXiv:0907.2582 [hep-th]] [Search INSPIRE].
[4] R. Gurau and J. P. Ryan, SIGMA **8**, 020 (2012) [arXiv:1109.4812 [hep-th]] [Search INSPIRE].
[5] J. Ambjørn, B. Durhuus, and T. Jonsson, Mod. Phys. Lett. A **6**, 1133 (1991).
[6] N. Sasakura, Mod. Phys. Lett. A **6**, 2613 (1991).
[7] M. Gross, Nucl. Phys. Proc. Suppl. **25A**, 144 (1992).
[8] N. Sasakura, Int. J. Mod. Phys. A **27**, 1250020 (2012) [arXiv:1111.2790 [hep-th]] [Search INSPIRE].
[9] N. Sasakura and Y. Sato, Phys. Lett. B **732**, 32 (2014) [arXiv:1401.2062 [hep-th]] [Search INSPIRE].
[10] N. Sasakura and Y. Sato, J. High Energy Phys. **1510**, 109 (2015) [arXiv:1506.04872 [hep-th]] [Search INSPIRE].
[11] N. Sasakura and Y. Sato, Prog. Theor. Exp. Phys. **2014**, 053B03 (2014) [arXiv:1401.7806 [hep-th]] [Search INSPIRE].
[12] N. Sasakura and Y. Sato, Prog. Theor. Exp. Phys. **2015**, 043B09 (2015) [arXiv:1501.05078 [hep-th]] [Search INSPIRE].
[13] A. Tanasa, arXiv:1512.02087 [hep-th] [Search INSPIRE].
[14] R. Gurau, Annales Henri Poincare **12**, 829 (2011) [arXiv:1011.2726 [gr-qc]] [Search INSPIRE].
[15] R. Gurau and V. Rivasseau, Europhys. Lett. **95**, 50004 (2011) [arXiv:1101.4182 [gr-qc]] [Search INSPIRE].
[16] V. Bonzom, R. Gurau, and V. Rivasseau, Phys. Rev. D **85**, 084037 (2012) [arXiv:1202.3637 [hep-th]] [Search INSPIRE].
[17] S. Dartois, R. Gurau, and V. Rivasseau, J. High Energy Phys. **1309**, 088 (2013) [arXiv:1307.5281 [hep-th]] [Search INSPIRE].
[18] V. Bonzom, R. Gurau, J. P. Ryan, and A. Tanasa, J. High Energy Phys. **1409**, 051 (2014) [arXiv:1404.7517 [hep-th]] [Search INSPIRE].
[19] J. Polchinski, *String Theory* (Cambridge University Press, Cambridge, 1998), Vol. 1.